Development of a Long-Range Lightning Detection Network for the Pacific: Construction, Calibration, and Performance*

ANTTI T. PESSI AND STEVEN BUSINGER

Department of Meteorology, University of Hawaii at Manoa, Honolulu, Hawaii

K. L. CUMMINS

The University of Arizona, Tucson, Arizona

N. W. S. DEMETRIADES, M. MURPHY, AND B. PIFER

Vaisala, Inc., Tucson, Arizona

ABSTRACT

The waveguide between the earth's surface and the ionosphere allows very low-frequency (VLF) emissions generated by lightning, called sferics, to propagate over long distances. The new Pacific Lightning Detection Network (PacNet), as a part of a larger long-range lightning detection network (LLDN), utilizes this attribute to monitor lightning activity over the central North Pacific Ocean with a network of ground-based lightning detectors that have been installed on four widely spaced Pacific islands (400–3800 km). PacNet and LLDN sensors combine both magnetic direction finding (MDF) and time-of-arrival (TOA)-based technology to locate a strike with as few as two sensors. As a result, PacNet/LLDN is one of the few observing systems, outside of geostationary satellites, that provides continuous real-time data concerning convective storms throughout a synoptic-scale area over the open ocean.

The performance of the PacNet/LLDN was carefully assessed. Long-range lightning flash detection efficiency (DE) and location accuracy (LA) models were developed with reference to accurate data from the U.S. National Lightning Detection Network (NLDN). Model calibration procedures are detailed, and comparisons of model results with lightning observations from the PacNet/LLDN in correlation with NASA's Lightning Imaging Sensor (LIS) are presented. The daytime and nighttime flash DE in the north-central Pacific is in the range of 17%–23% and 40%–61%, respectively. The median LA is in the range of 13–40 km. The results of this extensive analysis suggest that the DE and LA models are reasonably able to reproduce the observed performance of PacNet/LLDN.

The implications of this work are that the DE and LA model outputs can be used in quantitative applications of the PacNet/LLDN over the North Pacific Ocean and elsewhere. For example, by virtue of the relationship between lightning and rainfall rates, these data also hold promise as input for NWP models as a proxy for latent heat release in convection. Moreover, the PacNet/LLDN datastream is useful for investigations of storm morphology and cloud microphysics over the central North Pacific Ocean. Notably, the PacNet/LLDN lightning datastream has application for planning transpacific flights and nowcasting of squall lines and tropical storms.

1. Introduction and background

Lightning detection has great value for real-time storm tracking, warning, and nowcasting (e.g., Johnson et al. 1982; Demetriades and Holle 2005; Squires and Businger 2008). In remote regions where conventional data sources are not available, tracking of thunderstorms and assessing cyclone intensification are important challenges in weather prediction for civilian and military purposes. A lack of real-time weather data from the

areas surrounding naval aircraft carrier operations and civilian airports on islands presents an important opportunity for long-range lightning detection. In Hawaii and the surrounding Pacific region, there has been an unmet requirement for long-distance, real-time storm tracking that can now be met using modern ground-based long-range lightning location systems (LLSs).

Because of the long-range propagation characteristics of lightning electromagnetic signals in the very low-frequency (VLF) range, long-range LLSs provide cost-effective, accurate monitoring of convective storms over a synoptic-scale region. Thunderstorms over the ocean represent a threat to airborne carriers and ocean shipping and are mostly beyond the range of weather radars. Although geostationary satellites provide continuous infrared imagery, cirrus anvils often obscure convective activity. Some of the cirrus-obscured clouds pose little hazard to aircraft operations; however, convective clouds that produce lightning have significant updrafts, increasing the threat of turbulence and icing. Low orbiting satellites that carry microwave radiometers such as National Aeronautics and Space Administration's (NASA's) Earth Observing System (EOS) *Aqua* with its Advanced Microwave Scanning Radiometer for EOS (AMSR-E) and Tropical Rainfall Measuring Mission (TRMM) with its Microwave Imager (TMI) provide intermittent glimpses of convective precipitation. Unfortunately, the low and steeply inclined orbits of these satellites do not permit continuous monitoring of the evolution of convective weather systems.

The next-generation series of the Geostationary Operational Environmental Satellite (GOES) may carry geostationary lightning mappers (GLM; Christian 2006), which could monitor lightning continuously over a wide field of view. Until these instruments are in orbit, tested, and calibrated, ground-based lightning detection remains the only method to provide a continuous lightning datastream. The launch of the first GOES-R series satellite is scheduled for 2014.

In this paper, we describe the construction and instrumentation of the Pacific Lightning Detection Network (PacNet) and assess its observed performance and limitations. Furthermore, we describe the development of detection efficiency (DE) and location accuracy (LA) models and outline the derivation of the model parameters. Together, these are the necessary, initial steps toward the goal of quantitative applications of the lightning datastream, such as assimilation into NWP models.

a. Background: Very low-frequency signal propagation

Electromagnetic waves created by a lightning discharge radiate over a broad frequency range and prop-

agate in all directions. Very high-frequency (VHF) emissions occur during virgin electrical breakdown as well as during leader and streamer processes (Mazur et al. 1995; Shao and Krehbiel 1996). These signals can only be detected at ranges up to a few hundred kilometers since they rely on line-of-sight propagation and are not reflected by the ionosphere. The large current variations associated with return strokes in cloud-to-ground (CG) and very large pulses in cloud discharges are mainly observable in the VLF and low-frequency (LF) regions of the spectrum (Cummins et al. 1998a). When propagation distances are less than about 1000 km, significant energy in both the VLF and LF band can propagate as a ground wave, as shown in Fig. 1. At greater distances, energy in the VLF portion of the spectrum between 3 and 30 kHz (sferics) can propagate effectively in the waveguide defined by the earth's surface below and by the ionosphere above, specifically its lowest layer, the D region. Out to roughly 4000 km, most of the energy is carried in signals that can be accounted for using the first two "ionospheric hops" shown in Fig. 1. At even greater distances, propagation is more efficiently characterized using modal analysis (Wait 1968). Electron densities increase rapidly with height in the D region, typically from a few per cubic centimeters to a few hundred per cubic centimeters. VLF waves typically reflect from the heights of 60–75 km during the daytime when high electron densities extend into the lower ionosphere. During the night, the high electron density retreats to higher altitudes, with the reflections occurring in the range of 75–90 km.

Ionospheric D-region characteristics are often defined by two parameters: the reflection height h' and the exponential sharpness factor β [the rate of increase of electron density with height; Wait and Spies (1964)]. The parameter values are particularly stable during the day, resulting in predictable daytime wave propagation (Thomson 1993; McRae and Thomson 2000). The characteristics of the nighttime ionosphere are more variable, and the signal propagation is less predictable than by day. Thomson et al. (2007) measured the nighttime D-region parameters from the VLF phase and amplitude observations and found average midlatitude values of $h' = 85.1 \pm 0.4$ km and $\beta = 0.63 \pm 0.04$ km^{-1}. For daytime, McRae and Thomson (2004) found the value of h' varying between 58 and 71 km, and Thomson (1993) found an average value of $\beta = 0.45$ km^{-1}. Other factors, such as ground conductivity σ_g, ground permittivity, and ambient magnetic field, affect the VLF propagation. Attenuation rate is the lowest for $\sigma_g = \infty$, which is a good approximation for seawater (Wait 1968).
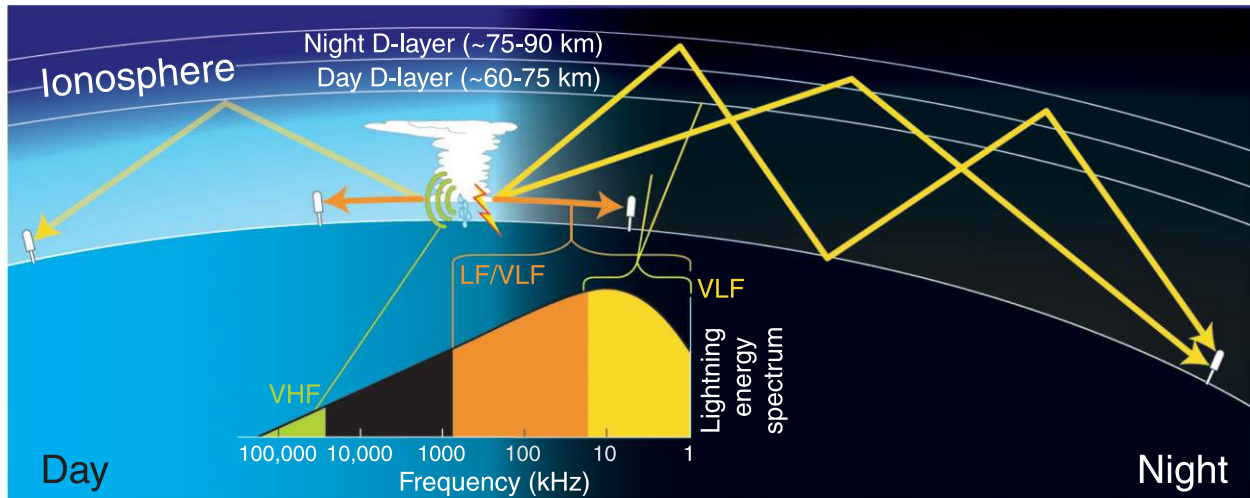
FIG. 1. Schematic diagram of the earth–ionosphere waveguide, which allows VLF (3–30 kHz) emissions from thunderstorms (sferics) to propagate thousands of kilometers through reflection. The best propagation is observed over the ocean at night.

Clilverd et al. (1999a) investigated lightning activity in Africa and South America from 10-kHz spectral power measurements using a VLF receiver in Halley, Antarctica. To investigate the significant diurnal and annual variations in the VLF propagation, they used signals from 10-kHz Omega transmitters in Liberia and Argentina. They found that during the austral winter, the signal strength in the Argentina–Halley path dropped quickly (in two hours) at 1100 UTC from its nighttime value of 1.0 to 0.6. The propagation factor in the Liberia–Halley path dropped quickly at 0600 UTC from 1.0 to 0.45, but it required six hours to reach its minimum value of 0.2. The annual variation in propagation factor varied between 1.0 in July and ~0.7 in January in both paths.

It is commonly known that eastward and westward propagating VLF waves have different propagation characteristics (e.g., Taylor 1960). The mean attenuation rate for subionospheric, westward propagating waves has been observed to be somewhat greater than for eastward propagation. Nickolaenko (1995) used VLF navigation system Omega at 10.2 kHz in the Atlantic and found attenuation rates of 2.1 dB Mm^{-1} for eastward propagation and 2.6 dB Mm^{-1} for westward propagation. Pappert and Hitney (1988) modeled nocturnal VLF signal propagation between Hawaii and San Diego and between Hawaii and Wake Island using empirical electron density profiles with ionospheric parameters of $\beta = 0.5$ km^{-1} and $h' = 87$ km. They compared the predictions to in-flight measurements and found that the predictability was much better for eastward propagation than for westward propagation. They argued that the propagation to the west is less stable and more sensitive to the variations in the ionosphere than propagation to the east. This is a second-order effect, which is not incorporated in the simple propagation models employed in this paper.

When the sunrise or sunset terminator crosses the propagation path, the situation becomes more complicated. A simple single-mode propagation theory is not sufficient, but multiple modes are required to explain the VLF propagation, as was noted by Budden (1961) and Wait (1962). Crombie (1964) modeled the effect of the sunrise terminator crossing over long VLF signal paths. He used a model with two waveguide modes and assumed a second mode in the nocturnal part of the path with significant mode conversion at the terminator. The terminator effect has been later discussed in many papers including Walker (1965), Ries (1967), Lynn (1967), and Pappert and Snyder (1972). Clilverd et al. (1999b) investigated 24-kHz signal propagation along a 12 000-km path from Cutler, Maine, to Faraday, Antarctica. The path was nearly parallel with the north–south meridian with only a 3° deviation from the meridian. They used five years of observations and the Naval Ocean Systems Center (NOSC) Long Wave Propagation Capability code (LWPC; Ferguson and Snyder 1990). The gross features of propagation were relatively well modeled. The timing of the amplitude minimum during the austral summer, in particular, was very well predicted, whereas the amplitude prediction was poorer.

Using the above body of knowledge, the approach taken in this paper will be to employ different model parameters for daytime and nighttime propagation that take into account diurnal changes in ionospheric

electron density and ground conductivity but that ignore the directional propagation effects. Since the propagation distances of interest are at or below 4000 km, analysis and results will be presented in terms of ground-wave and sky-hop propagation.

b. Long-range lightning location systems

Research systems exist that employ long-range lightning location methods with varying levels of performance and areas of coverage. The World Wide Lightning Location Network (WWLLN; Rodger et al. 2006) utilizes a time of group arrival (TOGA) method to locate lightning strikes. The Zeus long-range network (Chronis and Anagnostou 2003) uses an arrival time difference method. The Met Office employs the Arrival Time Difference Network (ATDNET; Nash et al. 2005; Keogh et al. 2006). Time of arrival methods typically need detection from three or four sensors to compute a strike location. PacNet sensors combine both magnetic direction finding (MDF) and time of arrival (TOA)-based methods and can locate a strike with as few as two sensors. We note that determining a location using ionospherically propagated signals seen by only two sensors will have somewhat larger location errors when compared to locations produced by three or more sensors. This is because polarization errors (due to nonhorizontal components of ionospherically propagated magnetic fields) can result in azimuth errors of several degrees.

2. Description of Pacific Lightning Detection Network

VLF sensors have been installed on four islands in the North Pacific Ocean: (i) Unalaska in the Aleutian Islands, Alaska; the Hawaiian Islands of (ii) Hawaii and (iii) Kauai; and (iv) Kwajalein in Marshall Islands (Fig. 2). PacNet sensors[1] are modified Improved Accuracy from Combined Technology/Enhanced Sensitivity and Performance (IMPACT/ESP) sensors designed for long-range detection (Figs. 3 and 4). The gain has been set to a high level to receive weak, ionospherically reflected sferics, and the bandwidth has been adjusted to have greatest sensitivity in the VLF band. The sensors use combined technology that employs both time of arrival and magnetic direction finding methods in the data processing (Cummins et al. 1998b).

These Pacific sensors work in combination with other Vaisala long-range lightning detection network (LLDN)
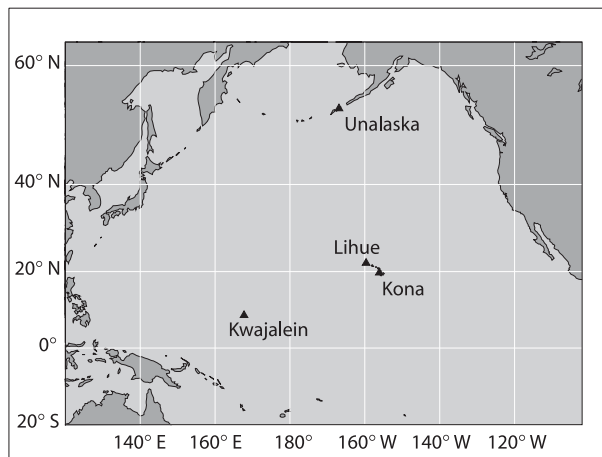

FIG. 2. Locations of four PacNet sensors installed at Unalaska, Lihue, Kona, and Kwajalein.

sensors, which consist of National Lightning Detection Network (NLDN) and Canadian Lightning Detection Network (CLDN) sensors located throughout the United States and Canada. The ~200 broadband LF/VLF sensors in these networks are not optimized for long-range detection but still provide important contributions to the overall network performance. The resulting long-range network, hereafter called PacNet/LLDN, continuously monitors lightning activity associated with convective storms across the central and eastern Pacific Ocean, north of the equator. Additional sites will be added in the near future, expanding the network to the western Pacific.

Although PacNet sensors are specifically designed for long-range detection, the concept of this "long-range lightning detection network" is broader than just these sensors, since the processing algorithm also incorporates sensor data from conventional sensors. The long-range location-processing algorithm identifies and accepts sensor data produced by both ground-propagated waves and ionospheric reflections that are rejected by the short-range algorithm used in NLDN and CLDN.

The raw (sensor) data from PacNet sites are transferred to Vaisala's Network Control Center in Tucson, Arizona, via the Internet, where they are processed in combination with the NLDN and CLDN sensor data. The strike locations and times are computed using the individual sensors' raw data, and final products are disseminated to users via the Internet.

3. Assessment of PacNet sensor performance

For quantitative applications of the PacNet/LLDN datastream, the DE and LA of the network must be

---

[1] We, hereafter, refer to the sensors installed on the Pacific islands as "PacNet sensors"and the sensors in North America as "conventional sensors,"although PacNet is a combination of both.
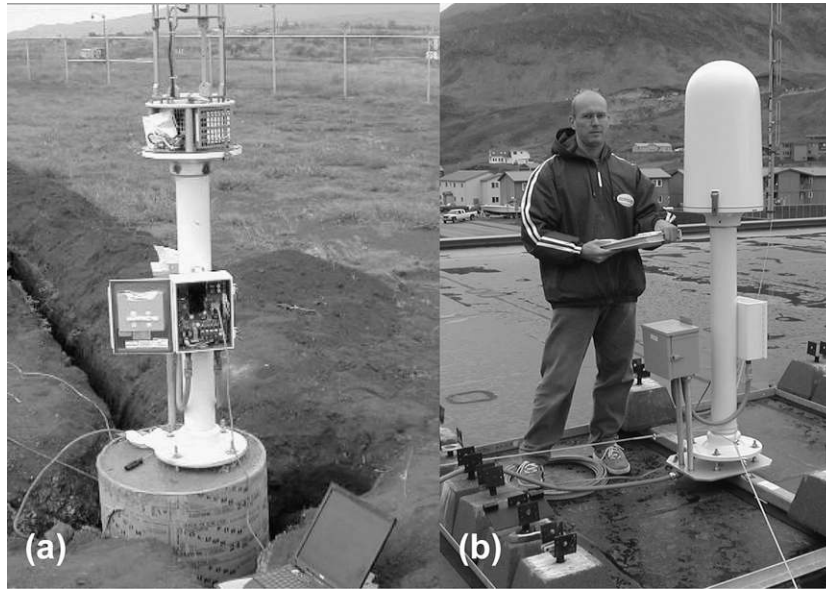
FIG. 3. (a) Installation stage at Lihue airport. The MDF loops are exposed at the top of the mast together with electric field and GPS antennas. Below them in the box is the main electronics module [primary line replaceable unit (PLRU)]. A laptop computer is connected to the sensor power/communication module (SPCM) to test the sensor. The power and communication cables are buried 90 cm below the surface. (b) Lead author with the finished installation at Unalaska.

assessed and then an accurate model of these characteristics constructed.

The percentage of lightning flashes reported by long-range lightning detection networks depends on the strength of the lightning discharge, solar angle, the distance between the lightning flashes and the sensors, specifics of the hardware, and the nature of the waveguide, which is discussed further in this section. This flash DE is defined as

$$\mathrm{DE}(x,y,t) = \frac{\text{number of flashes detected}}{\text{actual number of flashes}} \times 100\%.$$

$$(1)$$

The long-range LLS DE is generally best during the night and is poorest during the day. The lower-loss propagation at night is the result of improved ionospheric reflection (Fig. 1).

The LA is determined by the locations of sensors, the probability of detection by a specific group of sensors, and the time and angle error statistics (standard deviations) of the detected signals.

Basic sensor characteristics have been determined using data from a PacNet test sensor located in Tucson, Arizona, collected for one week in 2002. These data were compared to NLDN data collected during the same week in which a strong midlatitude storm system, with attendant squall lines, propagated from the high

plains across to the East Coast, providing robust lightning strike data from a range of distances.

The ionospherically reflected signals have different waveforms than typical ground waves produced by CG lightning return strokes (Fig. 5). Note the sharp initial downward peak and short peak-to-zero time for the ground wave at 264 km (Fig. 5a). At a distance of 860 km, Fig. 5b shows a distinct initial downward ground wave followed by a single-hop ionospheric reflection of opposite polarity (Kelso 1964). At a distance of 3400 km (Fig. 5c), the waveform is determined by multiple ionospheric components, but there is evidence of a very small initial downward ground wave, a slightly larger first-hop (inverted) sky wave (at $\sim$500 μs), and a larger downward second-hop sky wave (at $\sim$520 μs). Although this distant signal contains clear sky-hop components, its overall waveform would be best described using mode theory (Wait 1996). Since the field produced by a return stroke generally changes polarity at each reflection, the original polarity of the reflected waves cannot be readily determined, unless the ground wave is clearly identifiable.

The discharges detected by PacNet/LLDN are predominantly CG return strokes. Intracloud discharges have typically much weaker peak current than CG strokes and remain below the detection threshold. Ogawa and Brook (1964) reported typical current
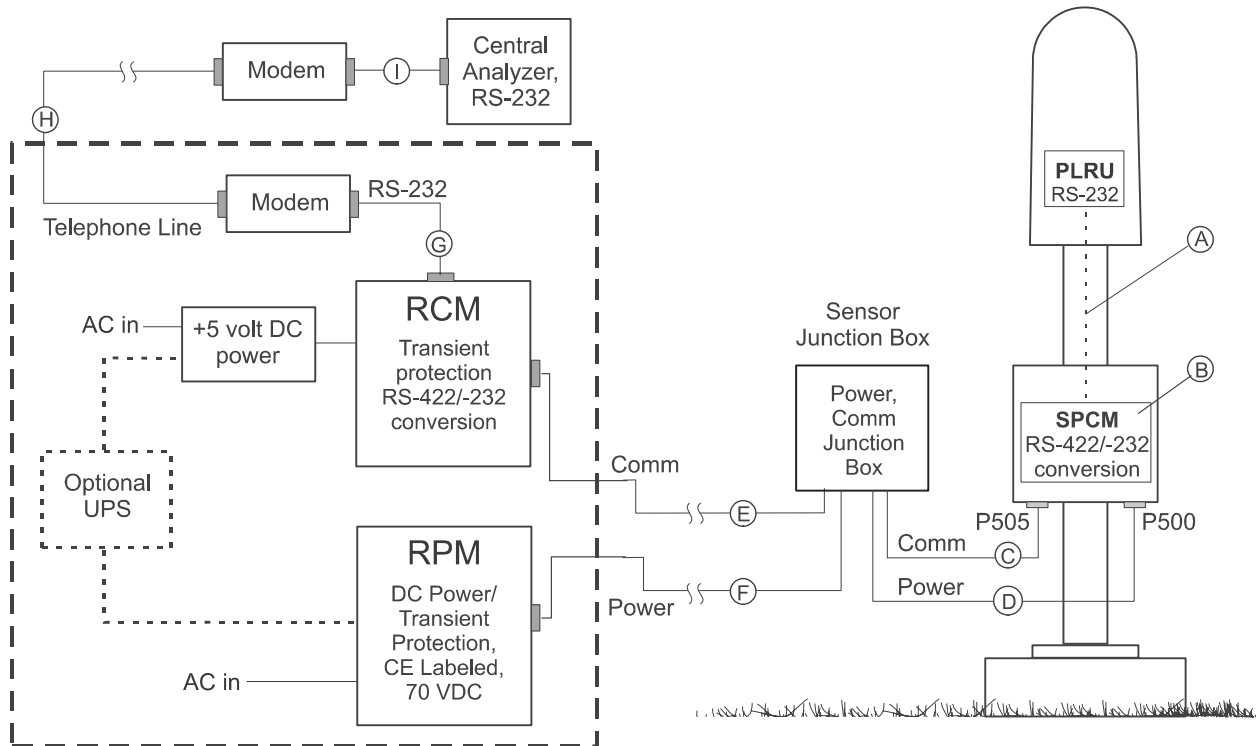
FIG. 4. IMPACT/ESP sensor schematic diagram showing the relationship between the remote communications module (RCM), the remote power module (RPM), the PLRU, and the SPCM. Legend: (A) RS-232, PLRU communication; (B) RS-422/-232 communication; (C) RS-422 communication; (D) sensor power; (E) RS-422 communication; (F) sensor power; (G) RS-232, 15-m maximum length; (H) telephone lines, 2- or 4-wire, leased line; and (I) RS-232, central analyzer communication.

amplitudes in cloud flashes of 1–4 kA. Murphy et al. (2006) used an LF sensor and the Lightning Detection and Ranging (LDAR) VHF lightning mapping system (Mazur et al. 1997) in Florida and observed that the majority (~70%) of all LF pulses from cloud discharges have amplitudes less than 1% (~0.2 kA) of the typical first return stroke (~20 kA) in a CG flash. Only the largest one to two pulses in each flash showed amplitudes equivalent to ~1 kA.

However, intracloud discharges can be sometimes accompanied by short duration, relatively high amplitude electric field change emissions, which are termed narrow bipolar pulses (NBPs; e.g., Smith et al. 1999). NBPs typically have much higher amplitude than the majority of cloud discharges [~70% of a typical CG return stroke; Smith et al. (1999)]. These events are relatively rare. Murphy et al. (2006) noted that NBPs constituted fewer than 1% of the cloud pulses. Smith et al. (2002) used the Los Alamos Sferic Array (LASA) and found that ~1.4% of the ~900 000 events located by the sferic array produced distinctive NBPs. Shao et al. (2006) used also LASA to investigate thunderstorms in Florida and found that among 34 000 flashes,

there were ~1.2% NBPs. These events are the subject of ongoing research.

a. Signal attenuation

As discussed in section 1, long-range propagation of sferics involves a complex interaction between the earth and the ionosphere. The behavior of this propagation medium varies with time of day, conductivity of the earth's path, and (to a lesser degree) season and direction. Since we are primarily interested in a "first order" characterization of propagation over saltwater, it is reasonable to simply partition propagation into two conditions: day and night. It has been shown that propagation characteristics between two widely separated locations (both attenuation and phase change as a function of frequency) transition fairly continuously from the daytime behavior to the nighttime behavior, over a period of two to three hours, as will be discussed later in this section.

The propagation characteristic that directly affects peak signal strength is the amplitude attenuation as a function of frequency and distance. This can be approximated by the expression
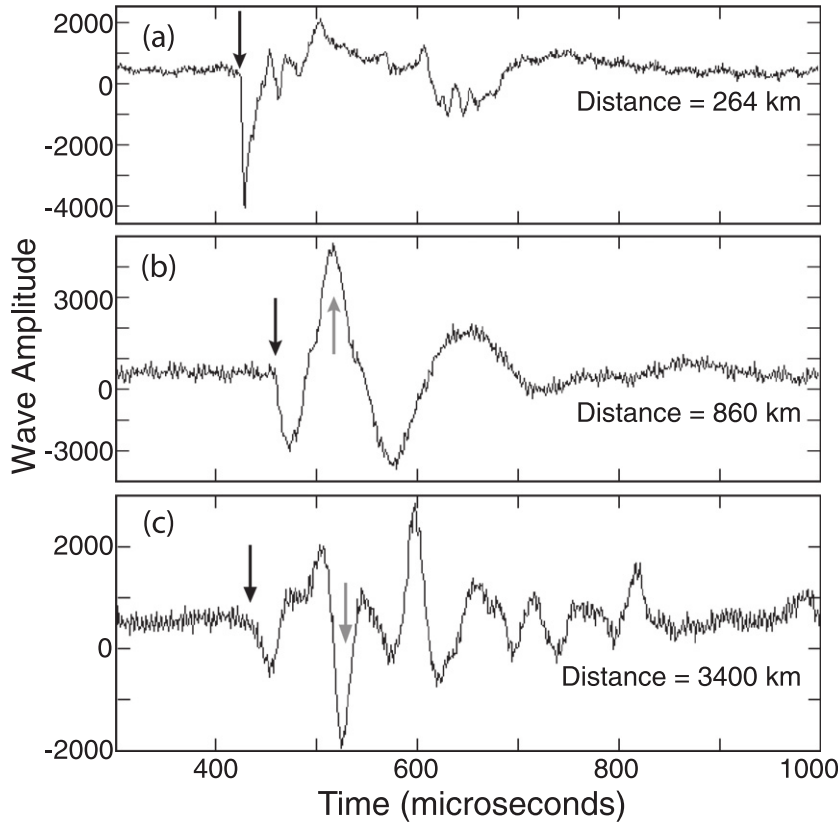
FIG. 5. (a)–(c) Vertical electric field waveforms for three different negative CG return strokes detected by sensors located at 264, 860, and 3400 km from the lightning stroke. The amplitude scale is uncalibrated. Black arrows indicate initial appearance of the ground wave. (b),(c) Gray arrows indicate the first-hop and second-hop reflected waves, respectively.

$$\text{Att} = \frac{\alpha_f}{R} \sqrt{\left[\frac{\theta}{\sin(\theta)}\right]} \exp\left(-\frac{R}{\lambda_f}\right). \qquad (2)$$

This attenuation function is a dimensionless scaling function, where α is a scaling constant; R is the distance along the earth's surface between the lightning discharge and a remote sensor; $\theta = R/R_e$; and R_e is the radius of the earth (Al'pert 1963, 245–248). The space constant (λ) or e-folding distance (the distance at which propagation losses reach $1/e$) is primarily dependent on the conductivity of the earth's portion of the path and the electron density profile in the atmosphere. This expression is a simplification of the general propagation models described by Wait (1968) and others, but empirical evidence suggests it captures the average behavior of broadband sferics over modest propagation distances (<4000 km).

The attenuation rate was derived by time-correlating data from the test sensor with NLDN data collected throughout the United States and comparing the loss-less signal strength (determined by the NLDN's estimated peak current and the known distance) with the peak field strength measured by the test sensor. The analysis of signal strength shows the expected exponential loss in energy with distance (Fig. 6), where the average relative field strength (filled circles) is normalized by the NLDN's estimated peak current. The standard deviation error bars show larger errors in the range of 2000–3500 km, where propagation involves a mix of ground and ionospheric propagation (see section 3b; Fig. 7). The daytime space constant shown in Fig. 6a is 10 000 km, and the nighttime space constant is 40 000 km (Fig. 6b).

The distinct separation of timing between ground, first-hop, and second-hop waves can be used to identify the wave type (Fig. 7). Within ~500 km of the sensor, nearly 100% of the signals are ground waves. Beyond that, the percentage of the first-hop waves increases sharply, whereas the ground-wave percentage decreases. They become equal at 900–1000 km. As noted earlier, the error bars for the observations of relative
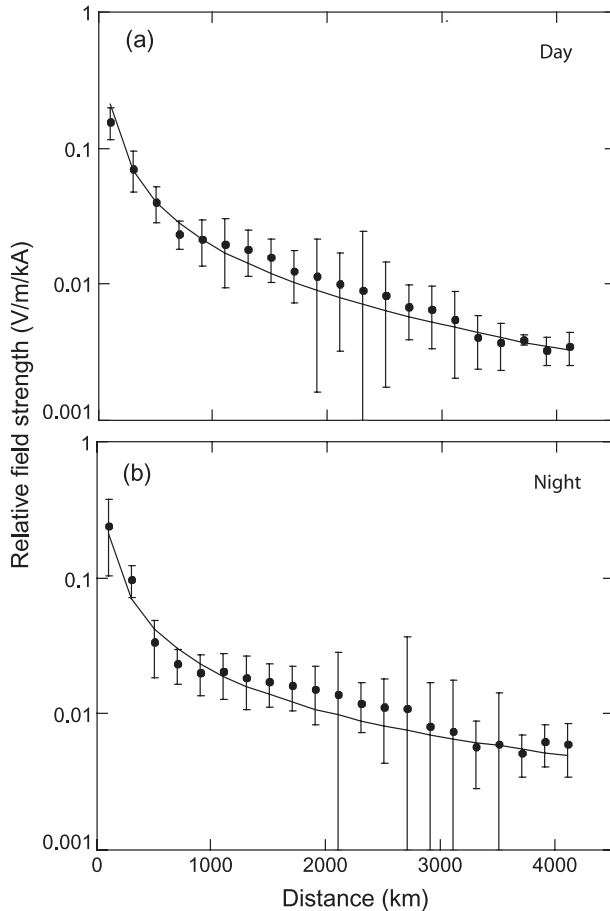
FIG. 6. Relative signal strength as a function of stroke distance as detected by a PacNet test sensor located in Tucson, AZ, for (a) day and (b) night. The error bars are ±1 standard deviation.
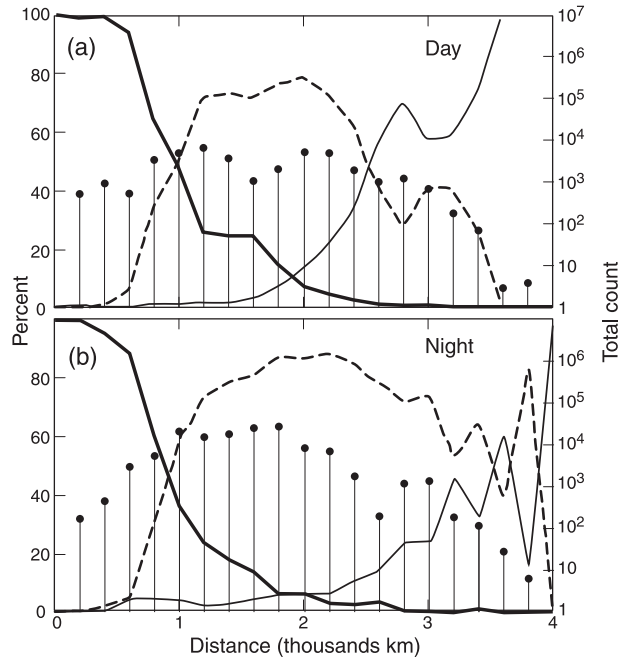

FIG. 7. Percentage of different propagation types as a function of distance for (a) day and (b) night. Thick solid line is for ground wave, dashed line for first-hop sky wave, and thin solid line for second-hop sky wave. The bars indicate the total number of strikes detected in each 200-km distance bin (right ordinate).

signal strength with distance are greatest at distances where there is significant overlap in the wave types (cf. Figs. 7 and 8). The addition of a signal processing capability within the sensor hardware to distinguish between the waveforms could reduce this uncertainty in the future.

b. Timing and angle errors

Timing errors were calculated by time-correlating data from the PacNet test sensor with NLDN data and comparing speed-of-light propagation time (determined from the NLDN stroke time and the known propagation distance) with the arrival time measured by the sensor (Fig. 8). These histograms were obtained by measuring the arrival time delay of PacNet sensor reports relative to NLDN-estimated stroke times measured with an accuracy of approximately one microsecond. All reports from one week of observations are included in this analysis. Figures 8a,c include reports with the same polarity as the NLDN peak current, and Figs. 8b,d include opposite-polarity reports. The polarity reversal (relative to the polarity determined by the NLDN) occurs when the earlier signal components (ground wave, first hop, and then second hop) fall below the fixed detection threshold of the sensor. The ground-wave signal delay distributions (average $\bar{x}$ and standard deviation σ) were nearly the same for day and night ($\bar{x} = 20.0$ μs, $\sigma = 5.0$ μs; and $\bar{x} = 19.3$ μs, $\sigma = 4.7$ μs, respectively; Figs. 8a,c). The first-hop sky-wave distribution shifted from daytime value of 52.9 μs ($\sigma = 4.7$ μs) to night value of 70.5 μs ($\sigma = 4.0$ μs; Figs. 8b,d). The second-hop distribution shifted from a daytime value of $\bar{x} = 90.0$ μs ($\sigma = 5.1$ μs) to night value of $\bar{x} = 104.0$ μs ($\sigma = 8.0$ μs; Figs. 8a,c). Note that the polarity reversal of the first hop helps distinguish it from the ground-wave and second-hop signals and that the signals delay distributions have almost no temporal overlap.

Angle errors were calculated by time-correlating data from the test sensor with NLDN data (150-μs time window) and comparing the true azimuth from the sensor (determined from the NLDN stroke location) with the azimuth measured by the sensor. An angle error histogram was derived from all time-correlated events with signal strengths from just above threshold to 4 times
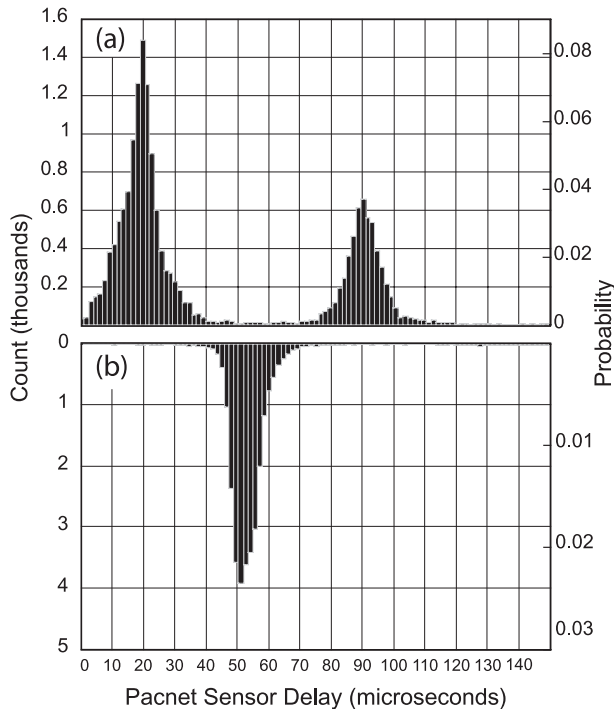
FIG. 8. (a) Daytime ground wave signal delay distribution is centered at 20.0 μs and has a standard deviation of 5.0 μs. Second-hop sky wave distribution is centered at 90.0 μs (σ = 5.1 μs). (b) First-hop (inverted) sky wave distribution is centered at 52.9 μs and has a standard deviation of 4.7 μs (graph inverted in reference to reversed polarity of first hop). (c) Nighttime average for ground-wave distribution is 19.3 μs (σ = 4.7 μs) and for second-hop distribution 104.0 μs with σ = 8.0 μs. (d) First-hop distribution is centered at 70.5 μs with σ = 4.0 μs (graph inverted in reference to reversed polarity of first hop).
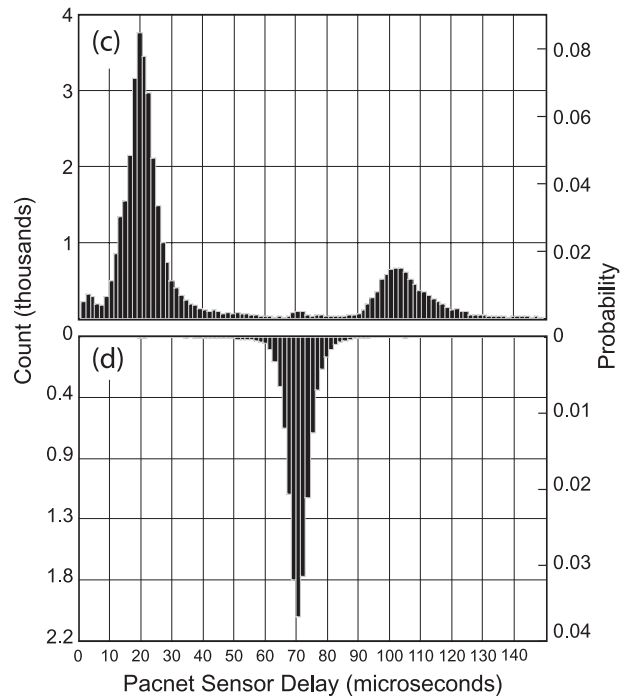
FIG. 8. (*Continued*)

threshold (Fig. 9). The parametric fit has a mean value of $-4°$ (resulting from an uncorrected antenna rotation and site errors due to local site conditions), and a standard deviation of 4.5°. This value is conservative, since it includes polarization errors and the variation of the local site error around its mean value.

c. Diurnal variation

As noted earlier, propagation characteristics between two widely separated locations (both signal attenuation and phase changes as a function of frequency) transition fairly continuously from the daytime to the nighttime behavior, over a period of two to three hours. This fact has been confirmed through analyses of arrival time delay and relative amplitude as functions of time of day for a portion of the PacNet sensor test period. For one 48-h observation period (hours 96–144), all lightning was at least 900 km from the test sensor (diamond symbols in Fig. 10). The plateau in the time delay time series (Fig. 10a) at ~50–55 μs reflects the behavior

during daytime propagation when the D layer extends lower in the ionosphere (e.g., Fig. 1). The plateau at ~70–75 μs reflects the behavior during nighttime propagation. Note the rapid and smooth transition between the two stable conditions that occurs during day–night transitions.

The PacNet "current" estimate (Fig. 10b) employed the propagation model in Eq. (2), using an attenuation rate of 10 000 km (representative for daytime propagation). This value is typically between 0.5 and 1.0, with random variations that can be larger than the day–night variability. The extent of these random variations is correlated with the variation in propagation distance, as one would expect. Note that for the hours 132–144, when most of the lightning is in the (narrow) range of 1500–2500 km, the random variability gets rather small. We note that this is the "sweet spot" range for one-hop propagation (see Figs. 7 and 8).

In addition, the behavior of PacNet DE during the transition periods between night and day over the Pacific was investigated, using the LLDN. Ground waves from flashes within 800 km of Hawaii were used as reference data. The two Hawaiian sensors detected these events, and the ground-wave propagation was assumed to have no diurnal variation. The same events detected by distant sensors (excluding Hawaii sensors) were assumed to be sky waves, since all other sensors
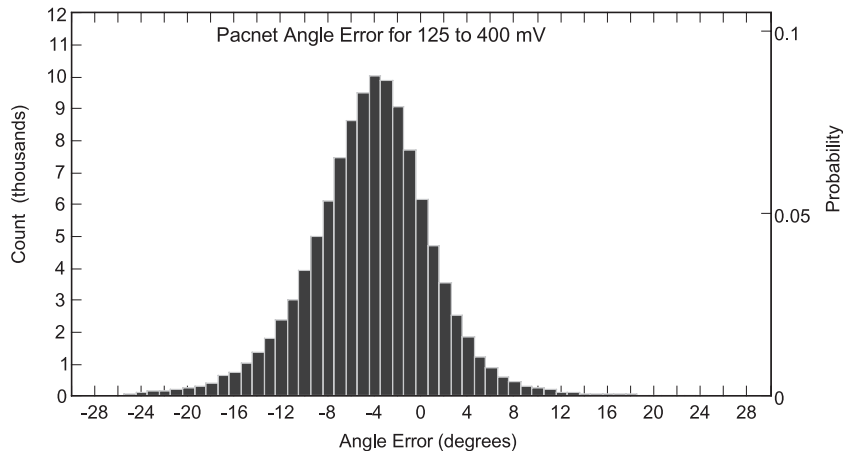
FIG. 9. Angle error without site error correction has a mean value of $-4.0°$ and a standard deviation of $4.5°$ (for both day and night).

were more than 2400 km away. Hourly relative DE values were obtained by comparing the number of sky wave events to the number of ground-wave events near Hawaii (Fig. 11). The diurnal variation of DE can be written as

$$DE_{d/n} = \frac{\frac{S_d}{G_d}}{\frac{S_n}{G_n}} = \frac{S_d}{G_d}\frac{G_n}{S_n}, \qquad (3)$$

where S and G are the number of flashes detected using sky waves and ground waves, respectively. The indices d and n refer to day and night, respectively.

In Fig. 11, the nighttime maximum DE begins to drop at ~0300 Hawaii local time, when the West Coast sensors are in dawn. The lowest DE is reached at 0600 LT, when the whole path from Hawaii to North America is in daylight. This continues until 1500 LT, when the North American sensors reach the dusk, and the DE starts to enhance. The maximum DE is reached at 1800 LT, when the whole propagation path is on the night side again. The relative DE during the day drops to ~20% of the night value. It should be noted that the diurnal variation shown in Fig. 11 over this test configuration area near Hawaii is close to its upper limit, as the nearest non-Hawaii sensors are >2400 km away. For quantitative applications of the PacNet datastream, such as numerical modeling, a linearly interpolated curve can be fit to the observed diurnal variation (see Fig. 11).

4. Modeling detection efficiency and location accuracy

As mentioned at the outset of section 3, quantitative applications require assessment of the DE and LA of the network, followed by construction of an accurate

model of these effects. A calibrated model of DE and LA allows these important parameters to be estimated throughout the domain of the network. As discussed in section 3, there are numerous factors that determine the DE of an LLS.

Specific examples of LLS DE are stroke DE_s (the fraction of all strokes, including first and subsequent) and subsequent stroke DE_{su} (excludes first strokes). Flash DE_f is unique in that a flash is reported (detected) if at least one stroke (first or subsequent) is detected. Therefore, flash DE_f can be much higher than any form of stroke DE.

In this section, the key parameters that determine the DE of individual sensors are defined, providing a framework for calculating DE for a given network geometry. This is followed by empirical derivation of the model parameters used to produce DE performance predictions for PacNet/LLDN.

The task of lightning detection begins with the electromagnetic field produced by the lightning discharge. In the case of CG lightning being detected at VLF/LF frequencies, the peak field strength (electric and/or magnetic) is roughly proportional to the peak current of the return stroke (Cummins et al. 1998b). The magnitude of the resulting field at a remote sensor location, which establishes the detectability of the signal by that sensor, is determined by three factors: (i) the attenuation of this field strength associated with normal propagation; (ii) additional losses due to finite conductivity along the propagation path; and (iii) imperfect (loss) ionospheric reflections. Once this attenuated signal reaches a remote sensor, it must exceed the detection threshold of the sensor, which is determined by sensor gain, threshold setting, and local noise. To obtain a location for the lightning discharge, the signal must be
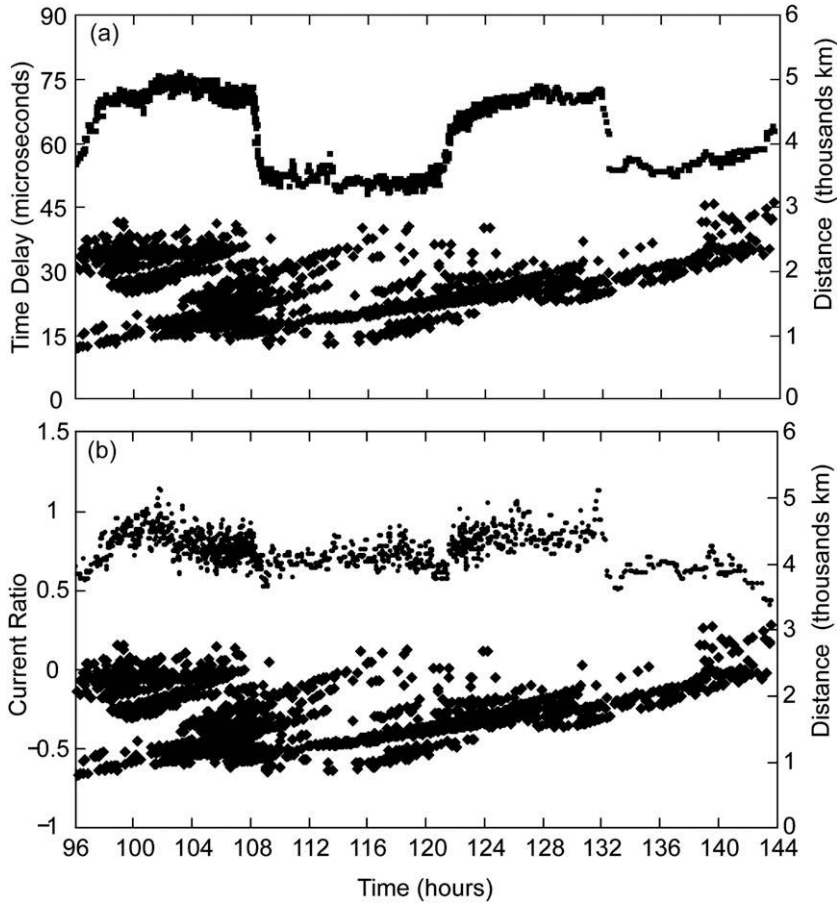
FIG. 10. Time series plots of (a) the variation of arrival time delay of VLF signals observed by the PacNet test sensor in Tucson, AZ, relative to UTC time of occurrence of the CG stroke determined by the NLDN. Each symbol represents the median value of nine time-ordered events. (b) Peak current estimated using the PacNet sensor magnetic field peak, relative to NLDN-estimated peak current. Diamonds in the lower part of each figure show the distance of the events from the sensor (right ordinate).
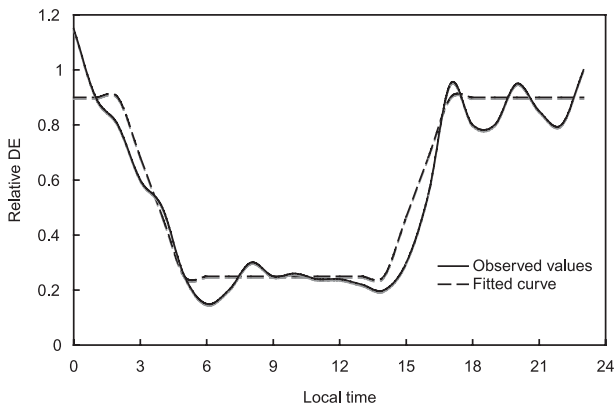

FIG. 11. Empirically derived diurnal DE variation over the North Pacific (solid line) and fitted curve used for diurnal DE correction (dashed line). Since the actual DE of ground-wave events is not exactly known, the DE scale (y axis) is relative.

seen by a sufficient number of sensors, which depends on strike point location (relative to the detecting sensors) and on the applied location method (MDF, TOA, or combined).

A graphical depiction of the detection process that is amenable to direct modeling is shown in Fig. 12. The first step involves the occurrence of a CG stroke with peak current I_0, selected from the probability distribution P_I (the peak current distribution). The peak electric and/or magnetic field produced by the stroke, having traveled a distance r_i, then reaches sensor S_i with incident signal SS_i. The probability of the sensor detecting this stroke is defined by the sensor DE function, illustrated in Fig. 12. Note that there is a minimum signal strength (detection threshold) below which no events are detected, and that the maximum detectability is not reached until the signal is a bit larger than the detection threshold. Note also that as signal strength increases
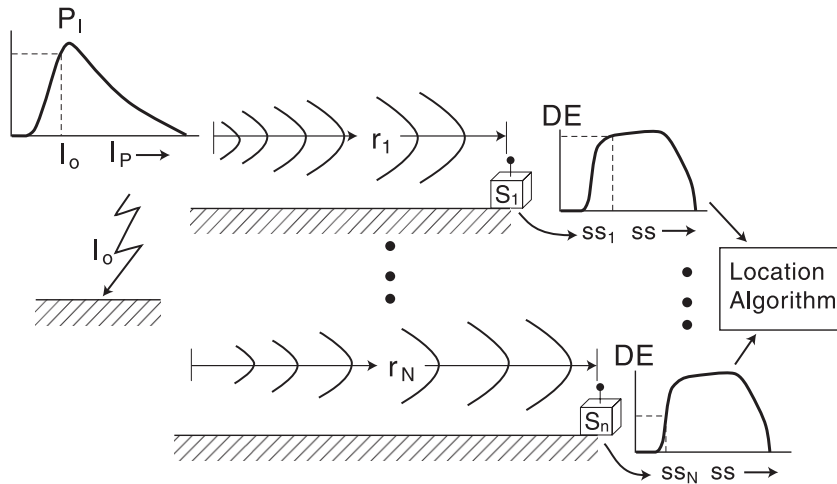
FIG. 12. Simplified schematic for LLS network detection efficiency. Here I_0 is the strike peak current, P_1 is the peak-current probability distribution, $r_1 \ldots r_n$ are the distance between the strike and the sensors $S_1 \ldots S_n$. $SS_1 \ldots SS_n$ are the incident signals at the sensors $S_1 \ldots S_n$. If the DE threshold is met, then the signal is passed on to a central location algorithm.

further, the DE decreases and eventually returns to zero when the sensor "over ranges" and is no longer able to provide reliable information. Since each sensor that detects a specific stroke will be at a different distance, they may all have different sensor DE values for this stroke. Using the assumption that each sensor responds independently from all other sensors, these DE values are independent for each sensor i. Using this assumption, and by defining the probability of sensor S_i not detecting the event as $Q_i(I_0) = 1 - DE_i(I_0)$, then the probability of a specific combination of sensors detecting the event is simply the product of the appropriate $P_i(I_0)$ and $Q_i(I_0)$ values for all sensors. For example, the probability P that a stroke with current I_0 is detected by a minimum of two sensors of a three-sensor network is

$$
\begin{aligned}
P = & [DE_1(I_0)*DE_2(I_0)*Q_3(I_0)] \\
& + [DE_1(I_0)*Q_2(I_0)*DE_3(I_0)] \\
& + [Q_1(I_0)*DE_2(I_0)*DE_3(I_0)] \\
& + [DE_1(I_0)*DE_2(I_0)*DE_3(I_0)].
\end{aligned} \tag{4}
$$

Using this construct, it is possible to determine the probability of detection for any specific number of sensors in a network of arbitrary size.

To produce a modeled overall DE estimate for a region, the region of interest is typically broken into a set of rectangular grid cells. For a point in the center of each cell, and for each possible peak current value, the model must determine the DE for each sensor. To determine the overall network detection efficiency for a specific peak current and grid point, one simply sums the probabilities for N or more sensors detecting a discharge, where N is the minimum number of sensors required by the network to locate a discharge. For networks that employ MDF in combination with TOA, N is two. For networks that employ direction finding by itself, N is 2 or 3, depending on the stroke location relative to the sensors locations. For networks that employ only the TOA method, N is 3 or 4. The overall DE is determined from the sum of DE values for each current value (I_0), weighted by their probability of occurrence taken from the peak current distribution P_i.

This general parametric model has been employed over the past 15 yr to estimate LLS performance. Recent validation of the model (for CG lightning detection in the United States involving ground-wave propagation paths) is provided in the work by Biagi et al. (2007).

To summarize, the fundamental information required to accurately model network DE is the distribution of peak currents, the detection threshold characteristics of the sensors, the propagation conditions (regional conductivity and ionospheric conditions), and knowledge of the location method (two, three, or four sensors required to get a location). The detection threshold characteristics of the sensor are strictly a function of the incident peak field strength and the gain of the sensor. The characteristics have been determined in a laboratory setting and confirmed in field tests performed by the sensor manufacturer (Vaisala). The location method employed in this network is the IMPACT method, which combines time of arrival and direction

finding, so only two sensors are required to detect a stroke for it to be reported by the network.

a. Estimation of DE model parameters for saltwater path

The form of the propagation model provided in Eq. (2) was shown to be a reasonable approximation of the observations from NLDN and a PacNet test sensor located in Arizona. To estimate DE for the LLDN, the two remaining parameters (peak current distribution and propagation characteristics; i.e., space constants) were needed for saltwater path conditions. These parameters were obtained by comparing recent information produced by the LLS operated by the Puerto Rico Electric Power Authority (PREPA) with information produced by the LLDN in the western Atlantic Ocean. The PREPA network is a short baseline network consisting of five low-gain IMPACT sensors installed in 2003. Using analyses performed by Vaisala, this network has a CG flash DE in excess of 95% over Puerto Rico and nearby surrounding waters and a median location error of 500 m or less. The western Atlantic portion of the LLDN operates with the same location algorithm configuration as the PacNet network in the Pacific, but this region is too distant from the four PacNet sensors to derive any value from them.

It has been shown (Orville and Huffines 2001) that the median peak current value for negative first strokes, inferred from LLS measurements, is somewhat larger when a stroke impacts saltwater than when it strikes ground. It is unknown whether this enhancement is the result of a change in the relationship between peak field and peak current over saltwater, or an actual increase in peak current in the channel. Either way, this effect produces a change in the population of "source" signals over saltwater that needs to be accounted for when estimating LLS DE over the oceans.

To account for this saltwater effect, the peak current distribution was constructed using negative first strokes obtained from the PREPA LLS for the calendar year 2006 (Fig. 13), obtained from the "sea" region surrounding Puerto Rico (Fig. 14c). A PREPA CG lightning stroke was considered to be detected by the LLDN if it occurred within 350 μs of the CG stroke detected by the PREPA network.

Since LLDN DE varies as a function of day and night, CG flash and stroke DE were computed as a function of peak current for both day and night. Daytime (nighttime) statistics were only computed between the hours of 1200 (0000) and 2200 (1000) UTC, when the propagation path between Puerto Rico and the LLDN sensors was all daylight (night), with no terminator crossing
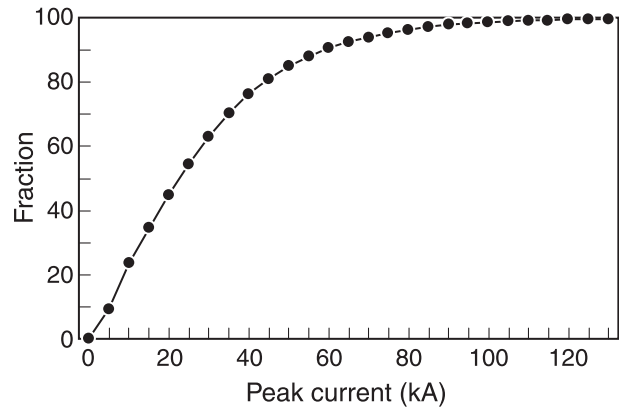

FIG. 13. Cumulative peak current distribution derived from CG first strokes striking salt water near Puerto Rico.

between Puerto Rico and LLDN sensors. LLDN DE was defined as the percentage of PREPA CG flashes (or strokes) detected by the LLDN. The observed flash DE values were 4.7% for day and 20.8% for night.

b. Refinement of DE model using Puerto Rico observations

The attenuation rates in the DE model [see Eq. (2)] were adjusted (2000-km space constant during the day and a 6000-km space constant for night), so that the predicted DE (~5% day and ~21% night) was consistent with the observed DE (Fig. 14), given the observed saltwater peak current distribution in the vicinity of Puerto Rico (Fig. 13). Note that these space constants are smaller than those observed for the PacNet test sensor, which reflects that lesser performance of the NLDN sensors.

The refined DE model was then applied to the PacNet/LLDN sensor distribution in the central North Pacific (Fig. 2), with the resulting predicted DE distribution shown in Fig. 15. In applying the refined DE model to Hawaii, it is assumed that the weather regime in the two locations, in a prevailing trade-wind belt, will produce similar peak current distributions. In this regard, it should be noted that during the period for which the Puerto Rico data were analyzed, no tropical cyclones passed through the region studied. In section 5a, comparison between observed and predicted DE in the vicinity of Hawaii are presented to test the validity of this assumption.

c. Modeling location accuracy

As described by Cummins et al. (1998b, their appendix) the median estimated location accuracy is defined as the semimajor axis of a location error ellipse. For the PacNet/LLDN LA model, the ellipse is computed
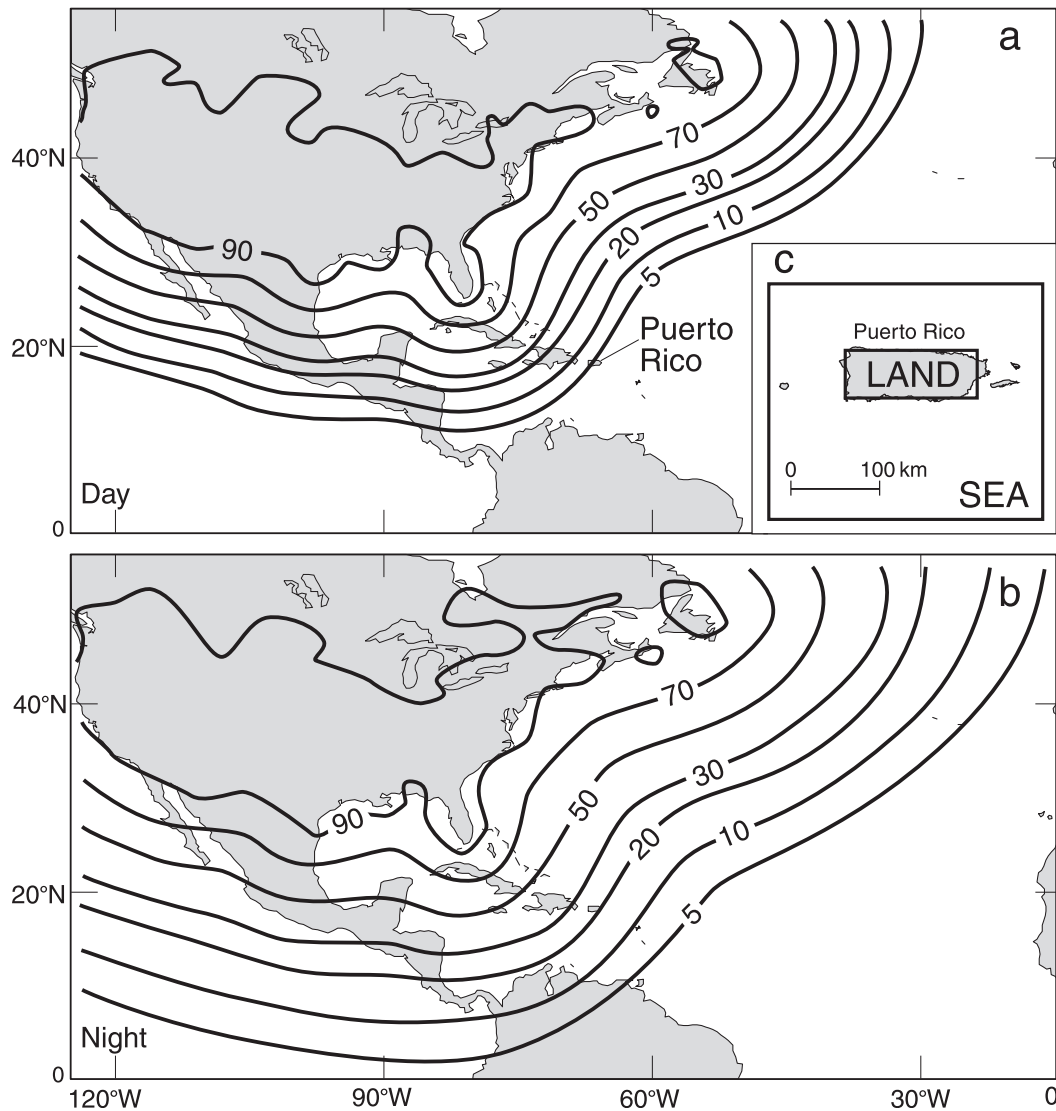
FIG. 14. Results from the DE model show (a) 5% day and (b) 20% night DE over Puerto Rico when using the reference peak current distribution and space constants of 2000 and 6000 km for day and night, respectively. (c) Lightning data analysis region for Puerto Rico. The saltwater region is the "sea" region, with the exclusion of the "land" region.

for each element of a 75 × 75 point grid and is determined by sensor locations, probability of detection by specific groups of sensors (DE model), and the time and angle standard errors. The timing and angle error characteristics were derived empirically using the Pac-Net test–sensor data, described in section 3. The errors were parameterized as the standard deviation of a normally distributed random variable (Figs. 8 and 9), resulting in a 5-μs RMS timing error value and an angle error of 4.5° RMS employed in the LA model.

The resulting modeled LA values are mostly between ~2 and 16 km between Hawaii and North America (Fig. 17). In the vicinity of Hawaii, the two Hawaiian sensors dominate the location accuracy in this DE-weighted LA model because the detection efficiency of the other sensors outside of Hawaii is much lower over this area. Although the distant sensors contribute slightly in the vicinity of Hawaii, the two Hawaii sensors detect the majority of the events. This two-sensor "subnetwork" exhibits the poorest LA near the exterior of the baseline defined by the two sensors (to the northwest and southeast), and the best LA when lines extending from the two sensors intersect at a 90° angle at the location of the lightning strike. In the immediate vicinity of Hawaii (northeast and southwest), the LA is relatively good but deteriorates away from the islands, as the detection
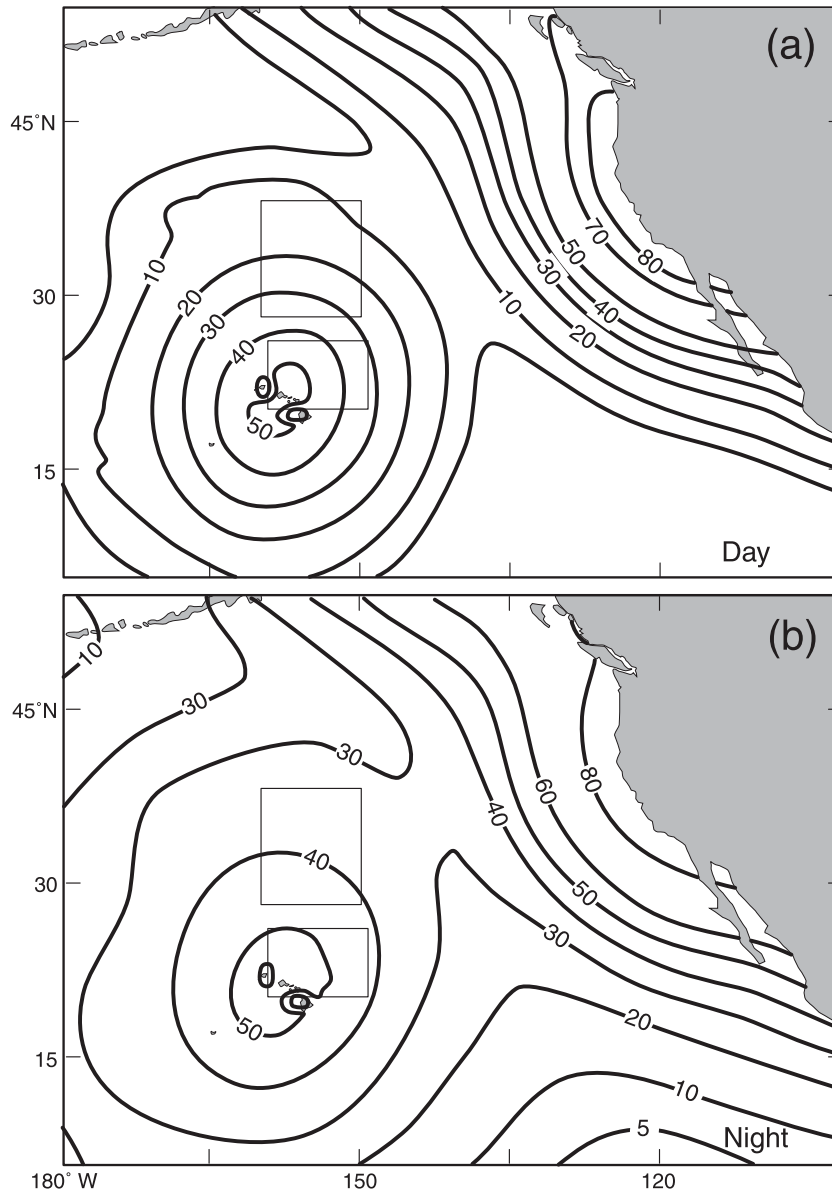
FIG. 15. Modeled DE (%) over the Pacific during (a) day and (b) night. The boxes show the areas where the observed DE was assessed. The observed values for the Hawaii region were 22% and 61% during the day and night, respectively. DE values for the central-north region were 19% and 44% for day and night, respectively.

angle becomes unfavorable. Farther to the northeast of Hawaii, the sensors from NLDN begin to detect flashes and the LA improves. The Kwajalein sensor improves the LA slightly to the southwest of Hawaii. Areas of the poorest LA occur to the southeast of Hawaii, near the extension of the baseline between the two Hawaii sensors. Furthermore, there are no additional sensors in that direction, nor does the area get any contribution from the other sensors, as a result of both the lower gain of the NLDN sensors and the applied hard limit of the

detection distance in the LA model (5000 km). To the northwest of Hawaii, Unalaska and Kwajalein improve the LA slightly, but the Hawaii sensors still dominate in the LA performance.

5. Observed performance of PacNet/LLDN

The performance of PacNet/LLDN was assessed using data from NASA's Lightning Imaging Sensor (LIS) onboard the TRMM satellite. Both DE and LA were

evaluated using time-correlated LIS flashes with Pac-Net/LLDN data. Three years of PacNet/LLDN data were used to assess the performance (DE and LA) of PacNet/LLDN over the central Pacific (February 2004–February 2007). Only days when at least three PacNet sensors (Unalaska, Lihue, and Kona plus LLDN) were up were included in the analysis. In addition, PacNet/LLDN data were filtered by removing multiple events. A single lightning strike is often detected as two or more PacNet/LLDN events. Multiple sky-wave locations are possible because more than one "collection" of sensors can experience a group-consistent propagation path delay. In contrast, there is only one (or zero) ground-wave location. The ground-wave events can usually be identified as the earliest event ($\sim$30–200 μs earlier), and the events in the region near Hawaii are only seen by two to three sensors. The time difference between LIS and LLDN events is determined by which "hop" triggered the sensor reports, the time of day, the distance between the sensors and the strike point, and the difference in the location calculation.

Location error (ΔD) results in a timing difference having a maximum of $\Delta D \times (3.3~\mu\text{s km}^{-1})$ and a minimum of zero, depending on the geometry of the network and the location errors. If we assume a maximum location error of 300 km, then the time difference is less than one millisecond. Expected time differences due to propagation alone are generally less than 200 μs. Time differences greater than one millisecond are probably different strokes in the flash, which can strike the ground up to 7–10 km away from the first stroke.

The LLDN stroke information includes three quality parameters. (i) Chi-square is the average-squared normalized angle and time deviations (from the optimized location) for the sensors that participated in each specific stroke location. This tells us if we have assumed reasonable angle and time deviations. In an ideal world, the mean and standard deviation for a large population of these values are 1.0. (ii) Error ellipse semimajor axis *(SMA, in km)* is the SMA of the error ellipse for the expected location error for each stroke, determined from the actual sensors reporting the stroke and their positions relative to the stroke location. This is also the parameter that we plot in our LA performance modeling—in that case, we normally assume that all sensors within a specified range will detect the stroke. This assumption is a problem for PacNet/LLDN, given the size of the network. Therefore, a special LA model was created that weighs each combination of two or more sensors by their DE (probability of occurrence). (iii) Average number of sensors reporting (NSR) is the average count of sensors that participated in the stroke location calculations. The minimum number is two (for

IMPACT sensor networks). When there is a large NSR, either the DE is quite high or only high-current strokes are located at a great distance from the sensors. The spatial distribution of this value gives insight into the actual behavior of the network. When more than one LLDN stroke location is time correlated with a LIS flash, the above error statistics are applied to select between multiple PacNet/LLDN locations.

a. Observed detection efficiency

The DE over the central Pacific was tested over two areas: near Hawaii (20–26°N, 149–159°W) and over the central-north region (28–38°N, 150–160°W; Fig. 15). The total number of LIS and PacNet/LLDN flashes occurring over the grid cells were counted over the 3-yr period, February 2004–February 2007. Both day and night DE were assessed. Day (night) data include all the flashes occurring between 0900 and 1500 (2100–0300) LT over each grid cell. The 6-h time windows centered at midnight and noon were selected to avoid terminator effects in the propagation path.

Three different corrections were applied to LIS data to make the PacNet/LLDN and LIS flash rates comparable: (i) LIS data were DE-corrected using values of 0.73 for day and 0.93 for night, according to Boccippio et al. (2002); (ii) LIS view time is a function of latitude, thus the flash rates were normalized for view time over the selected areas; and (iii) LIS reports were corrected for an estimated IC:CG ratio since LIS detects both intracloud (IC) and CG flashes, whereas the strikes detected by PacNet/LLDN are predominantly CG (section 3).

Since no high-quality lightning data are available over the central North Pacific, data from the PREPA LLS, described in section 4, were used to estimate the IC:CG ratio. Although Puerto Rico is in a different basin than PacNet, PREPA provided suitable high-quality lightning data for determining the IC:CG ratio over the subtropical ocean. No tropical cyclone activity occurred near Puerto Rico during the period of the dataset, making the data representative of the tradewind regime that characterizes both Puerto Rico and Hawaii.

The IC:CG ratio was assessed using all days in 2006 during which there were at least three LIS flashes detected over the high-quality lightning data region provided by the PREPA. Only the flashes occurring over the ocean were included in the analysis. There were a total of 29 days and 347 LIS flashes that met these criteria. Each LIS flash was classified as either an IC or CG flash. An LIS flash was classified as a CG flash if it occurred within ±100 ms of a PREPA CG flash (first stroke time; LIS flash duration was considered, i.e., within 100 ms of the beginning or end of a LIS flash). To

be classified as a CG flash, a LIS flash also had to occur within 15 km of a PREPA CG flash. Two LIS flashes could not be classified as CG if they both met these criteria for only one PREPA flash (i.e., when a LIS flash was classified as a CG flash, that PREPA CG flash was consumed and not used again for classifying any other LIS flashes). In addition, when multiple PREPA flashes matched one LIS flash, duplicate PREPA events were removed. This analysis yielded an oceanic IC:CG ratio of 4.8, which was used to normalize the LIS flash rates for the PacNet/LLDN DE estimation over the Hawaii region.

Previous studies have shown a weak correlation between IC:CG ratio and latitude, with IC:CG decreasing with increasing latitude (Pierce 1970; Prentice and Mackerras 1977; Mackerras et al. 1998;). Therefore, we used a IC:CG ratio of 4.0 over the central-north region (28°–38°N) to normalize the LIS flash rates. This value is consistent with the aforementioned studies.

Using the above approach, the DE over the Hawaii region was calculated to be 22% during the day and 61% at night. The DE over the central-north region varied between 19% during the day and 44% at night (Fig. 15).

The issue of infrequent LIS sampling was addressed using a 10% data deprivation study, also known in statistics as the jackknife method (e.g., Efron 1981). The PacNet/LLDN and LIS data were divided into 10 similarly sized parts that were matched temporally. The DE was computed 10 times, with one part of the data omitted during each computation. This yielded a mean DE for the Hawaii region of 23% for day and 61% for night with standard deviations of 4% and 7%, respectively. For the central-north region, the mean DE was 22% for day and 45% for night with standard deviations of 12% and 7%, respectively. Compared to the computations with the original full dataset, these values are within 1% for the Hawaii region and within 3% for the central-north region.

It is possible that LIS will miss more CG flashes than cloud discharges as a result of the lower height of illuminated channels in the clouds, as suggested by Boccippio et al. (2001) for Optical Transient Detector (OTD). This issue was assessed by determining the number of PREPA CG flashes occurring within ±5 s of a LIS flash but which were not consumed by the tighter time correlation test discussed above. These flashes set a conservative bound on the number of CG flashes missed by LIS. This method yielded a slightly reduced IC:CG ratio of 4.4 and DE values of 21% for day and 57% for night over the Hawaii region. Using a reduced IC:CG ratio of 3.5 for the central-north region, the DE values were 17% and 40% for day and night, respectively.

The observed DE of 17%–22% for day and 40%–45% for night over the central-north region is in relatively good agreement with the DE model (Fig. 15), although the variation is large for daytime using the jackknife method. Over the Hawaii region, the observed DE of 21%–23% for day is lower than modeled, and the observed DE of 57%–61% for night is higher than modeled (Fig. 15). It is suggested that the underestimate of the daytime DE is because of partial blockage of ground waves by high terrain to the north and east of the Kona sensor. Slightly higher DE at night may simply be a reflection of the longer space constants that characterize the performance of the PacNet sensors in Hawaii.

b. Observed location accuracy

The LA is defined as the difference between the actual flash location and the location the LLS observes. The location accuracy of PacNet/LLDN was assessed using LIS data. The LIS flash location is an optical centroid with nadir and limb resolutions of 4 and 6 km, respectively. Therefore, the results from the LA analysis need to be interpreted cautiously, considering the resolution of LIS data. The great-circle distances between all the PacNet/LLDN and LIS flashes occurring within ±1-ms time window were computed. The time stamp in the LIS flash data is not corrected for transmitting delay, resulting in 2-ms bias in the dataset (D. Boccippio 2007, personal communication). Therefore, PacNet/LLDN events were temporally matched with LIS flashes that occurred within a 1–3-ms-lagged time window of the LIS time stamp. The SMA and chi-values represent the quality of the location, and if there are multiple locations within 1 ms, the flash with the smallest value of $SMA/\sqrt{\chi}, (\chi \geq 1)$ is chosen to represent the flash location. As the number of matching pairs was relatively small, LA was averaged over relatively large grid boxes to obtain a reasonable sample size. All the boxes were located between 25° and 38°N, with "east," "central," and "west" box boundaries of 140°–155°W, 155°–165°W, and 165°–180°W, respectively. The median observed location accuracies over the east, central, and west boxes were 13, 35, and 40 km, respectively (see Fig. 16). Although the data points are relatively evenly distributed over the boxes, the modeled LA does vary within each box, especially within the west box. Therefore, the median modeled LA over each box was computed by taking the median of the modeled LA at each of the locations of the lightning strikes inside each box. The LA model has 1.2° latitude × 2.0° longitude grid spacing. The median modeled location accuracies over the east, central, and west boxes were 12, 11, and 67 km, respectively.
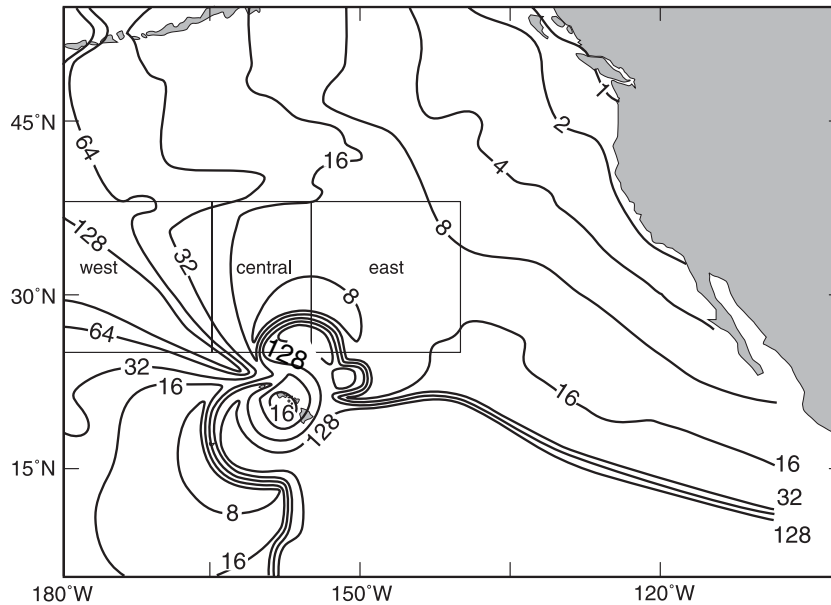
FIG. 16. Modeled LA (km) of PacNet/LLDN with four PacNet sensors located in Unalaska, Kwajalein, Lihue, and Kona (+ LLDN). The boxes show the areas where the observed LA was assessed.

Calibration of PacNet/LLDN includes the calculation of site error corrections. Site errors are systematic angle errors caused by the scattering of the received signals in the vicinity of the sensors (e.g., Krider et al. 1976; Hiscox et al. 1984). The calibration process relies on redundant information in the form of additional lightning sensors or an independent measurement source. Given that there are currently four PacNet sensors in the North Pacific and only two sensors in Hawaii (Lihue and Kona), existing site error corrections are challenging. Therefore, in the vicinity of Hawaii, lightning strikes near the baseline between the two Hawaii sensors may have large location errors when only these two sensors detect the discharge. By contrast, strikes away from the baseline can be accurately located, especially if additional sensors outside Hawaii participate in the detection. Strikes detected with more than two sensors are less sensitive to site errors as a result of the nature of the combined direction finding and time-of-arrival methods (Cummins et al. 1998b). In practice, the favorable geometry afforded by the large number of U.S. and Canadian sensors helps to reduce the location errors over the eastern Pacific near the coast of North America.

6. Summary, conclusions, and discussion

The waveguide between the earth's surface and the ionosphere allows VLF emissions generated by light-ning to propagate over long distances. PacNet, as a part of a larger long-range lightning detection network (LLDN), utilizes this attribute to monitor lightning activity over the central North Pacific Ocean with a network of ground-based lightning detectors that have been installed on four widely spaced (400–3800 km) Pacific islands. PacNet/LLDN sensors combine both magnetic direction finding (MDF) and time-of-arrival (TOA)-based technology to locate a strike with as few as two sensors. As a result, the PacNet/LLDN is one of the few observing systems, outside of geostationary satellites, that provide continuous real-time data concerning convective storms throughout a synoptic-scale area over the open ocean (Figs. 17 and 18).

The detection efficiency and location accuracy of PacNet/LLDN varies with time of the day and the location of the thunderstorm with respect to the sensors. Detection efficiency and location accuracy models have been developed and applied to quantify the lightning rates and locations over the North Pacific region. The model parameters were derived by comparing the waveforms arriving at a PacNet test sensor to NLDN lightning data from throughout the continental United States. Lightning data from Puerto Rico were then used in conjunction with LLDN data to derive the saltwater peak current distribution and space constants for the DE model.

The LIS data were used to assess the location accuracy and detection efficiency of PacNet/LLDN. The
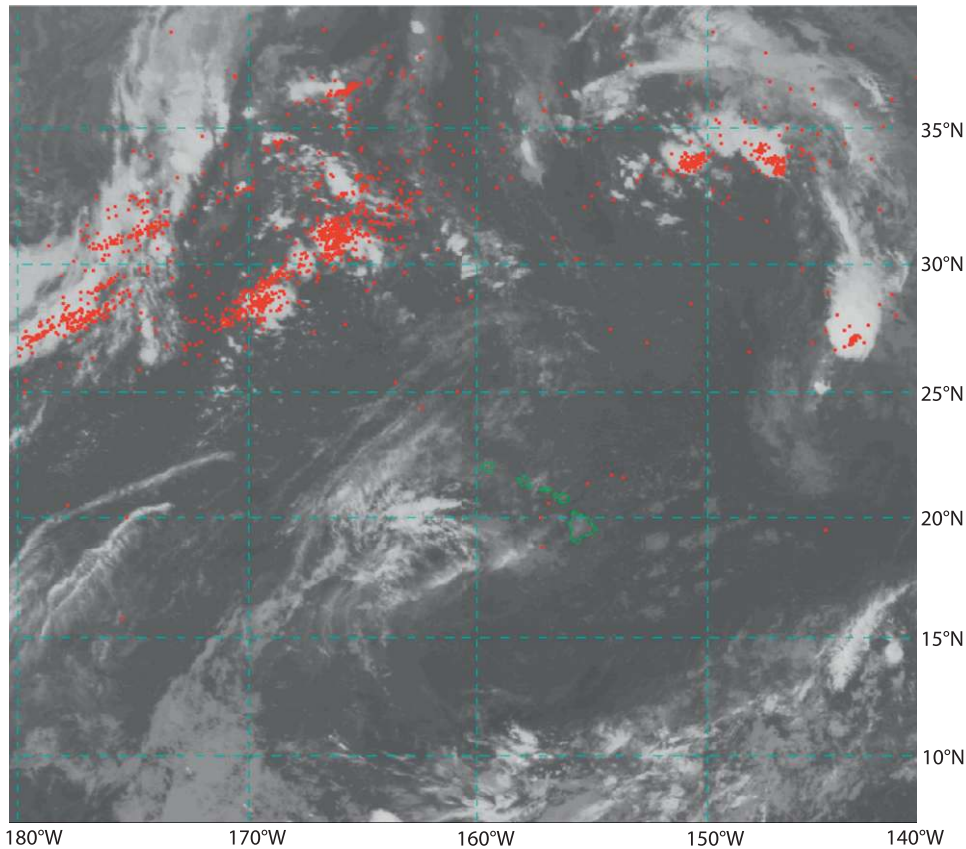
FIG. 17. PacNet/LLDN lightning data (red dots) overlaid on *GOES-10* infrared satellite image at 1000 UTC on 3 Sep 2004. The image shows lightning active convective storms on the transpacific air traffic routes between the West Coast and Hawaii. Areas of intense lightning can be used to differentiate between cold cirrus and deep convection. Note that the effect of inferior network geometry on the LA west of 160°W longitude is apparent in the image.

observed location accuracy was in the range of 13–40 km over the central North Pacific, in reasonable agreement with the LA model. The observed detection efficiency over the central-north region was 17%–22% and 40%–45% for day and night, respectively. These values were in good agreement with the DE model. In the vicinity of Hawaii, the observed DE was 21%–23% and 57%–61% for day and night, respectively. These values differ 10%–20% from the modeled values. These discrepancies may be due to unmodeled partial blocking of ground waves by terrain during the day and the fact that the space constants associated with PacNet and NLDN sensors differ. As the geometry of the network evolves with the addition of new sensors, network DE and LA will be reevaluated in future.

Discussion: Applications of PacNet/LLDN data

Thunderstorms pose a variety of hazards to aviation and marine interests, including high winds, wind shear, microbursts, turbulence, icing, heavy precipitation, and lightning strikes. In remote regions where conventional weather data are sparse and satellite data are either infrequent or unrevealing, tracking of thunderstorms, squall lines, and developing cyclones are important challenges in weather prediction for civilian and military purposes. Long-range lightning data from PacNet/LLDN are not only useful in the planning of transoceanic flight routes and in the development of optimum ship tracks for ocean voyages but also for assessing the potential for intensification in tropical and extratropical cyclones (e.g., Price et al. 2007).

The results of a detailed analysis effort suggest that the lightning–rainfall relationship is relatively robust over the central-north Pacific Ocean (e.g., Pessi and Businger 2009). These results hold promise for use of the PacNet/LLDN datastream as a proxy for latent heat release in deep convective clouds. Studies have shown that the assimilation of lightning data into numerical weather prediction models leads to improved initialization and better forecasts, particularly in the short
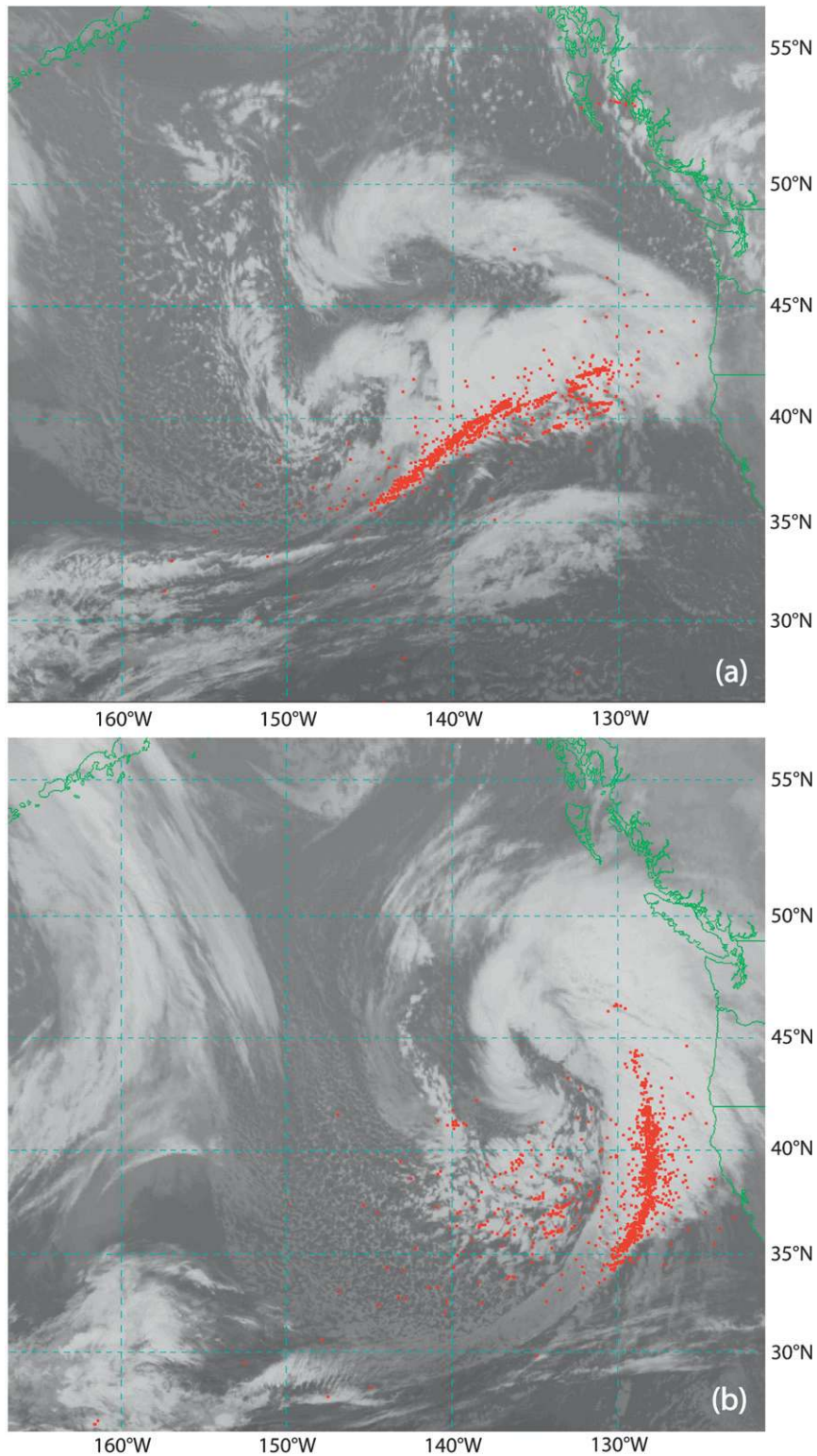
FIG. 18. A strong winter storm over the eastern Pacific Ocean at (a) 1230 UTC on 18 Dec 2002 and (b) 0630 UTC 19 Dec 2002. Long-range lightning data (red dots) occurring ± 30 min from the time the image are overlaid on *GOES-10* infrared satellite images.

term (Alexander et al. 1999; Chang et al. 2001; Papadopoulos et al. 2005; Pessi et al. 2006).

Long-range lightning sensors represent a mature, low-maintenance technology. Given the promising results obtained to date through the analysis of the PacNet/LLDN datastream (e.g., Squires and Businger 2008; Pessi et al. 2006), plans are being developed for Pacific-wide coverage by an expanded network of sensors. Additional sensors will increase overall detection efficiency while improving the location accuracy of an expanded PacNet/LLDN.

REFERENCES

Alexander, G. D., J. A. Weinman, V. M. Karyampudi, W. S. Olson, and A. C. L. Lee, 1999: The effect of assimilating rain rates derived from satellites and lightning on forecasts of the 1993 Superstorm. *Mon. Wea. Rev.,* **127,** 1433–1457.

Al'pert, Ya. L., 1963: *Radio Wave Propagation and the Ionosphere.* Consultants Bureau Enterprises, 394 pp.

Biagi, C., K. Cummins, K. Kehoe, and E. Krider, 2007: National Lightning Detection Network (NLDN) performance in southern Arizona, Texas, and Oklahoma in 2003–2004. *J. Geophys. Res.,* **112,** D05208, doi:10.1029/2006JD007341.

Boccippio, D. J., K. L. Cummins, H. J. Christian, and S. J. Goodman, 2001: Combined satellite- and surface-based estimation of the intracloud–cloud-to-ground lightning ratio over the continental United States. *Mon. Wea. Rev.,* **129,** 108–122.

——, W. J. Koshak, and R. J. Blakeslee, 2002: Performance assessment of the Optical Transient Detector and Lightning Imaging Sensor. Part I: Predicted diurnal variability. *J. Atmos. Oceanic Technol.,* **19,** 1318–1332.

Budden, K. G., 1961: *The Wave-Guide Mode Theory of Wave Propagation.* Prentice-Hall, 325 pp.

Chang, D.-E., J. A. Weinman, C. A. Morales, and W. S. Olson, 2001: The effect of spaceborne microwave and ground-based continuous lightning measurements on forecasts of the 1998 Groundhog Day Storm. *Mon. Wea. Rev.,* **129,** 1809–1833.

Christian, H. J., 2006: Geostationary Lightning Mapper (GLM). Preprints, *12th Conf. on Aviation Range and Aerospace Meteorology*, Atlanta, GA, Amer. Meteor. Soc., J2.3. [Available online at http://ams.confex.com/ams/Annual2006/techprogram/paper_105471.htm.]

Chronis, T. G., and E. N. Anagnostou, 2003: Error analysis for a long-range lightning monitoring network of ground-based receivers in Europe. *J. Geophys. Res.,* **108,** 4779, doi:10.1029/2003JD003776.

Clilverd, M. A., N. W. Watkins, A. J. Smith, and K. H. Yearby, 1999a: Diurnal and annual variations in 10-kHz radio noise. *Radio Sci.,* **34,** 933–938.

——, N. R. Thomson, and C. J. Rodger, 1999b: Sunrise effects on VLF signals propagating over a long north–south path. *Radio Sci.,* **34,** 939.

Crombie, D. D., 1964: Periodic fading of VLF signals received over long paths during sunrise and sunset. *J. Res. Natl. Bur. Stand., Sect. D,* **68,** 27–34.

Cummins, K. L., E. P. Krider, and M. D. Malone, 1998a: The US National Lightning Detection Network™ and applications of cloud-to-ground lightning data by electric power utilities. *IEEE Trans. Electromagn. Compat.,* **40,** 465–480.

——, M. J. Murphy, E. A. Bardo, W. L. Hiscox, R. D. Pyle, and A. E. Pifer, 1998b: A combined TOA/MDF technology upgrade of the U.S. National Lightning Detection Network. *J. Geophys. Res.,* **103,** 9035–9044.

Demetriades, N. W. S., and R. L. Holle, 2005: Long-range lightning applications for hurricane intensity. Preprints, *Conf. on Meteorological Applications of Lightning Data*, San Diego, CA, Amer. Meteor. Soc., P2.8.

Efron, B., 1981: Nonparametric estimates of standard error: The jackknife, the bootstrap and other methods. *Biometrika,* **68,** 589–599.

Ferguson, J. A., and F. P. Snyder, 1990: Computer programs for assessment of long-wavelength radio communications, version 1.0: Full FORTRAN code user's guide. Naval Ocean Systems Center Tech. Doc. 1773, Defense Tech. Information Center AD-B144 839.

Hiscox, W. L., E. P. Krider, A. E. Pifer, and M. A. Uman, 1984: A systematic method for identifying and correcting "site errors" in a network of magnetic direction finders. Preprints, *Int. Aerospace and Ground Conf. on Lightning and Static Electricity,* Orlando, FL, National Interagency Coordination Group, 7-1–7-5.

Johnson, R. L., D. E. Janota, and J. E. Hay, 1982: An operational comparison of lightning warning systems. *J. Appl. Meteor.,* **21,** 703–707.

Kelso, J. M., 1964: *Radio Ray Propagation in the Ionosphere.* McGraw-Hill, 408 pp.

Keogh, S., E. Hibbett, J. Nash, and J. Eyre, 2006: The Met Office Arrival Time Difference (ATD) system for thunderstorm detection and lightning location. Met Office Forecasting Research Tech. Rep. 488, 22 pp.

Krider, E. P., R. C. Noggle, and M. A. Uman, 1976: A gated, wideband magnetic direction finder for lightning return strokes. *J. Appl. Meteor.,* **15,** 301–306.

Lynn, K. J. W., 1967: Anomalous sunrise effects observed on a long transequatorial VLF propagation path. *Radio Sci.,* **2,** 521–530.

Mackerras, D., M. Darveniza, R. Orville, E. Williams, and S. Goodman, 1998: Global lightning: Total, cloud and ground flash estimates. *J. Geophys. Res.,* **103,** 19791–19809.

Mazur, V., P. R. Krehbiel, and X. M. Shao, 1995: Correlated high-speed video and radio interferometric observations of a cloud-to-ground lightning flash. *J. Geophys. Res.,* **100** (D12) 25731–25753.

——, E. Williams, R. Boldi, L. Maier, and D. Proctor, 1997: Initial comparison of lightning mapping system with operational time-of-arrival and interferometric systems. *J. Geophys. Res.,* **102,** 3311–3325.

McRae, W. M., and N. R. Thomson, 2000: VLF phase and amplitude: Daytime ionospheric parameters. *J. Atmos. Sol. Terr. Phys.,* **62,** 609–618.

——, and ——, 2004: Solar flare induced ionospheric D-region enhancements from VLF phase and amplitude observations. *J. Atmos. Sol.-Terr. Phys.,* **66,** 77–87.

Murphy, M. J., N. W. S. Demetriades, R. L. Holle, and K. L. Cummins, 2006: Overview of capabilities and performance of the U.S. National Lightning Detection Network. Preprints, *12th Conf. on Aviation Range and Aerospace Meteorology,* Atlanta, GA, Amer. Meteor. Soc., J2.5. [Available online at http://ams.confex.com/ams/pdfpapers/103980.pdf.]

Nash, J., N. C. Atkinson, E. Hibbett, G. Callaghan, and P. L. Taylor, 2005: Progress in introducing new technology sensor sites for the Met Office long-range lightning detection system. *Proc. WMO Tech. Conf. on Meteorological and Environmental Instruments and Methods of Observation (TECO-2005),* Bucharest, Romania, World Meterological Organization, 2.9.

Nickolaenko, A. P., 1995: ELF/VLF propagation measurements in the Atlantic during 1989. *J. Atmos. Sol.-Terr. Phys.,* **57,** 821–834.

Ogawa, T., and M. Brook, 1964: The mechanism of the intracloud lightning discharge. *J. Geophys. Res.,* **69,** 5141–5150.

Orville, R. E., and G. R. Huffines, 2001: Cloud-to-ground lightning in the United States: NLDN results in the first decade, 1989–98. *Mon. Wea. Rev.,* **129,** 1179–1193.

Papadopoulos, A., T. Chronis, and E. N. Anagnostou, 2005: Improving convective precipitation forecasting through assimilation of regional lightning measurements in a mesoscale model. *Mon. Wea. Rev.,* **133,** 1961–1977.

Pappert, R. A., and F. P. Snyder, 1972: Some results of a mode-conversion program for VLF. *Radio Sci.,* **7,** 913–923.

——, and L. R. Hitney, 1988: Empirical modeling of nighttime easterly and westerly VLF propagation in the earth-ionosphere waveguide. *Radio Sci.,* **23,** 599–611.

Pessi, A., and S. Businger, 2009: Relationships between lightning, precipitation, and hydrometeor characteristics over the North Pacific Ocean. *J. Appl. Meteor. Climatol.,* in press.

——, ——, and T. Cherubini, 2006: Comparison of two methods for assimilation of lightning data into NWP models. Preprints, *First Int. Lightning Meteorology Conf.,* Tucson, AZ, Vaisala, 12 pp.

Pierce, E., 1970: Latitudinal variation of lightning parameters. *J. Appl. Meteor.,* **9,** 194–195.

Prentice, S., and D. Mackerras, 1977: The ratio of cloud to cloud-ground lightning flashes in thunderstorms. *J. Appl. Meteor.,* **16,** 545–549.

Price, C., Y. Yair, and M. Asfur, 2007: East African lightning as a precursor of Atlantic hurricane activity. *Geophys. Res. Lett.,* **34,** L09805, doi:10.1029/2006GL028884.

Ries, G., 1967: Results concerning the sunrise effect of VLF signals propagated over long paths. *Radio Sci.,* **2,** 531–538.

Rodger, C. J., S. Werner, J. B. Brundell, E. H. Lay, N. R. Thomson, R. H. Holzworth, and R. L. Dowden, 2006: Detection efficiency of the VLF World-Wide Lightning Location Network (WWLLN): Initial case study. *Ann. Geophys.,* **24,** 3197–3214.

Shao, X.-M., and P. R. Krehbiel, 1996: The temporal development of intracloud lightning. *J. Geophys. Res.,* **101** (D21), 26641–26668.

——, Stanley, M., A. Regan, J. Harlin, M. Pongratz, and M. Stock, 2006: Total lightning observations with the new and improved Los Alamos Sferic Array (LASA). *J. Atmos. Oceanic Technol.,* **23,** 1273–1288.

Smith, D. A., and Coauthors, 1999: A distinct class of isolated intracloud lightning discharges and their associated radio emissions. *J. Geophys. Res.,* **104** (D4), 4189–4212.

——, K. B. Eack, J. Harlin, M. J. Heavner, A. R. Jacobson, R. S. Massey, X. M. Shao, and K. C. Wiens, 2002: The Los Alamos Sferic Array: A research tool for lightning investigations. *J. Geophys. Res.,* **107,** 4183, doi:10.1029/2001JD000502.

Squires, K., and S. Businger, 2008: The morphology of eyewall lightning outbreaks in two category 5 hurricanes. *Mon. Wea. Rev.,* **136** 1706–1726.

Taylor, W. L., 1960: VLF attenuation for east-west and west-east daytime propagation using atmospherics. *J. Geophys. Res.,* **65,** 1933.

Thomson, N. R., 1993: Experimental daytime VLF ionospheric parameters. *J. Atmos. Terr. Phys.,* **55,** 173–184.

——, M. A. Clilverd, and W. M. McRae, 2007: Nighttime ionospheric *D* region parameters from VLF phase and amplitude. *J. Geophys. Res.,* **112,** A07304, doi:10.1029/2007JA012271.

Wait, J. R., 1962: *Electromagnetic Waves in Stratified Media.* Pergamon Press, 372 pp.

——, 1968: Recent theoretical advances in the terrestrial propagation of VLF electromagnetic waves. *Advances in Electronics and Electron Physics,* L. Marton, Ed., Vol. 25, Academic Press, 145–210.

——, 1996: *Electromagnetic Waves in Stratified Media.* Electromagnetic Wave Theory Series, IEEE/Oxford University Press, 372 pp.

——, and K. P. Spies, 1964: Characteristics of the earth-ionosphere waveguide for VLF radio waves. National Bureau of Standards Tech. Note 300.

Walker, D., 1965: Phase steps and amplitude fading of VLF signals at dawn and dusk. *J. Res. Natl. Bur. Stand., Sect. D.,* **69,** 1435–1443.